Available online at www.sciencedirect.com
SCIENCE DIRECT
Journal of Catalysis 240 (2006) 1–7
JOURNAL OF CATALYSIS
www.elsevier.com/locate/jcat

Comparative study on redox properties of nanosized CeO_2 and CuO/CeO_2 under CO/O_2

A. Martínez-Arias [a,*], D. Gamarra [a], M. Fernández-García [a], X.Q. Wang [b], J.C. Hanson [b], J.A. Rodriguez [b,*]

[a] *Instituto de Catálisis y Petroleoquímica, CSIC, C/Marie Curie 2, Campus Cantoblanco, 28049 Madrid, Spain*
[b] *Chemistry Department, Brookhaven National Laboratory, Upton, NY 11973, USA*

Received 7 December 2005; revised 17 February 2006; accepted 21 February 2006

Available online 29 March 2006

Abstract

Nanosized CeO_2 and CuO/CeO_2 samples, active for CO-PROX or related processes were comparatively examined by O_2 probe electron paramagnetic resonance and in situ Raman and X-ray diffraction techniques. Their behavior toward CO reduction, as well as the oxygen-handling properties of the CO-reduced samples, was explored. An appreciable reduction of the ceria bulk was detected on treatment under CO at 473 K. On the basis of the analysis of the evolution of different oxygen-derived species (superoxide, peroxide, O^-) on low-temperature (77–300 K) oxygen chemisorption on the CO-reduced samples, a general picture of the redox properties of the samples is presented. Results demonstrate that the presence of copper promotes completion of the redox cycle under CO/O_2 by favoring both ceria reduction and oxidation. This can be relevant to explaining the remarkable oxidation activity and synergetic effects observed for catalysts combining CuO and CeO_2.

Keywords: Copper oxide; Ceria; Catalyst; CO Oxidation; CO-PROX; Water–gas shift; Redox properties; Electron paramagnetic resonance; In situ Raman; In situ X-ray diffraction

1. Introduction

Catalysts based on ceria present a wide range of applications, including three-way catalysts for automobile exhaust gas emission control, removal of SO_x–NO_x from fluid catalytic cracking flue gases, electrocatalysts over fuel cell electrodes, and catalysts for various oxidation and hydrogenation reactions [1–4]. For most of these applications, ceria-related compounds are thought to operate mainly as redox facilitators or structural promoters of the active metal (or metal oxides) with which they are in contact, as well as a bifunctional promoter [1,2]. A noteworthy aspect of ceria-related oxides is that they can promote the activity of catalysts with different functionalities, such as precious metals (e.g., Rh, Pt, and/or Pd, typically present in TWC) and base metals or metal oxides [1,2,5–13].

Among the latter, outstanding activities, comparable to those exhibited by precious metal catalysts, are shown by copper (or copper oxide) catalysts for reactions of high technological interest, including common CO oxidation and preferential CO oxidation in H_2-rich streams (CO-PROX), methanol steam reforming, methanol synthesis from CO and H_2, and the water–gas shift [5–17]. For most of these reactions, redox changes are thought to be most relevant to understanding the catalytic properties of the systems [2]. Particularly in CO oxidation or related reactions (e.g., CO-PROX), the catalytic features are generally explained on the basis of a Mars and van Krevelen redox-type mechanism, in which redox changes can occur in both the copper oxide and ceria components (and/or the corresponding interface) [7,16,17]. This is supported, in general terms, by the correlation observed between redox properties (in terms of the behavior toward reduction/oxidation under CO/O_2) and CO oxidation catalytic activity, which appears to be maximized for configurations of copper oxide and ceria (or structurally related oxides) in which CuO-type clusters are strongly dispersed on

* Corresponding authors.
E-mail addresses: amartinez@icp.csic.es (A. Martínez-Arias), rodrigez@bnl.gov (J.A. Rodriguez).

0021-9517/$ – see front matter
doi:10.1016/j.jcat.2006.02.026

the ceria support [5–17]. However, details on the respective specific role of each oxide component (or of the interfacial region as a whole) and/or the nature of the species active in these processes are, to the best of our knowledge, still lacking.

On the other hand, recent contributions have shown (mainly from an experimental standpoint) that the use of nanostructured configurations of the cerium oxide component can provide new catalytic properties (beyond a simple intrinsically associated specific area increase) to these materials that can be beneficial for this type of reaction [18–20]. This can be related to structural or electronic modifications produced in the nanostructured oxides [21], which in the case of ceria can be related to the presence of reduced states of cerium (mainly at the surface or close to surface positions) and/or to their higher redox activity [22–26].

Within this context, the present work aims to provide further insight into redox processes occurring in these nanostructured oxide catalysts on interaction with CO/O_2. For this purpose, redox changes induced on reduction under CO and subsequent oxidation with O_2 were analyzed with electron paramagnetic resonance (EPR) and in situ Raman spectroscopy, and in situ X-ray diffraction (XRD) was used to complement the analysis of the reduction under CO. Given the characteristics of these techniques, this work focuses mainly on the ceria part of the systems and also aims to complement previous detailed examinations of the redox properties of the copper component in the CuO/CeO_2 catalyst [7,27].

2. Experimental methods and preliminary characterization

2.1. Materials

The CeO_2 support was prepared by precipitation within a reverse microemulsion. For this, two microemulsions of similar characteristics containing aqueous phases prepared by dissolving cerium(III) nitrate hexahydrate for the first and tetramethylammonium hydroxyde pentahydrate for the second were mixed, with *n*-heptane as an organic solvent, Triton X-100 (Aldrich) as a surfactant, and hexanol as a co-surfactant in the microemulsions. After centrifugation, decanting, and rinsing with methanol, the resulting solid was dried at 383 K for 24 h and finally calcined under air at 773 K for 2 h. Details of the preparation parameters used in the synthesis of this support were similar to those described previously for related materials [28]. Previous investigation of this CeO_2 support by XRD and HREM found multifaceted, more or less rounded nanocrystals with the fluorite phase and a relatively narrow size dispersion (average size, 7.7 nm; standard deviation, ca. 2 nm). The nanocrystals were shown to form polycrystalline aggregates in the micron size, and the sample displayed $S_{BET} = 101\ m^2\,g^{-1}$ [27,29].

The copper oxide catalyst supported on CeO_2 (CuO/CeO_2) was prepared by incipient wetness impregnation of the CeO_2 support using an aqueous solution of $Cu(NO_3)_2{\cdot}3H_2O$ (to give a final copper load of 1 wt%, representing ca. 157 μmol of Cu per g of catalyst). The resulting material was dried overnight at 383 K and subsequently calcined under air at 773 K for 2 h. Textural and bulk structural characteristics of this sample were close to those of the parent CeO_2 support [27]. In turn, XPS and XAFS showed that most of the copper appeared on the ceria surface mainly as highly dispersed CuO-type clusters after calcination at 773 K under diluted oxygen (more details below) [27]. Such a configuration of components (obtained for the copper loading used for this sample) has been shown to yield optimum catalytic properties in CO oxidation and other related processes [17].

2.2. Techniques

EPR spectra were recorded at 77 K with a Bruker ER 200 D spectrometer operating in the X-band and calibrated with a DPPH standard ($g = 2.0036$). Samples of about 30 mg were placed inside a quartz probe cell with greaseless stopcocks using a conventional high-vacuum line (capable of maintaining a dynamic vacuum of ca. $6 \times 10^{-3}\ N\,m^{-2}$) for the different treatments. In all cases, the sample was pretreated in 300 Torr ($1\ Torr = 133\ N\,m^{-2}$) of pure oxygen at 773 K for 2 h. CO reduction treatments at a specific reduction temperature were made under static conditions using 100 Torr of CO, heating for 1 h at the corresponding temperature, and subsequently outgassing at the same temperature for 0.5 h. Quantitative estimation of the amount of species present in the spectra was performed by double-integration of the corresponding EPR spectra and comparison with a copper sulfate standard. Computer simulation was used to determine spectral parameters and determine specific contributions of signals to a determinate spectrum.

Raman spectra were collected using a single monochromator Renishaw System 1000 equipped with a cooled CCD detector and holographic super-notch filter. The samples were excited with the red laser line (632.8 nm, He–Ne laser); the spectral resolution was ca. 3 cm^{-1}, and spectrum acquisition consisted of two accumulations with a total acquisition time of ca. 10 min. An in situ cell (Linkam, TS-1500) that enables thermal treatment under flowing gas was used to hold the samples in powder form. The as-prepared samples were pretreated in flowing 20% O_2/He at 773 K for 1 h before any further treatment. The reduction treatment was performed under flowing CO at 473 K, and subsequent reoxidation was done at room temperature under 20% O_2/He flow. All of the spectra were recorded at room temperature after (when required) allowing cooling under the corresponding oxidizing/reducing atmosphere used for the respective treatments.

XRD experiments were carried out on beamline X7B ($\lambda = 0.922$ Å, $Q \leqslant 6\ Å^{-1}$) of the National Synchrotron Light Source (NSLS) at Brookhaven National Laboratory. The as-received sample was loaded into a sapphire capillary cell that was attached to a flow system [30,31]. A small resistance heater was wrapped around the capillary, and the temperature was monitored with a 0.1-mm chromel–alumel thermocouple that was placed in the capillary near the sample. Two-dimensional powder patterns were collected with a Mar345 image plate detector, and the powder rings were integrated using the FIT2D code [32]. In situ diffraction patterns were collected during redox treatments under diluted O_2/CO. These reactions were car-

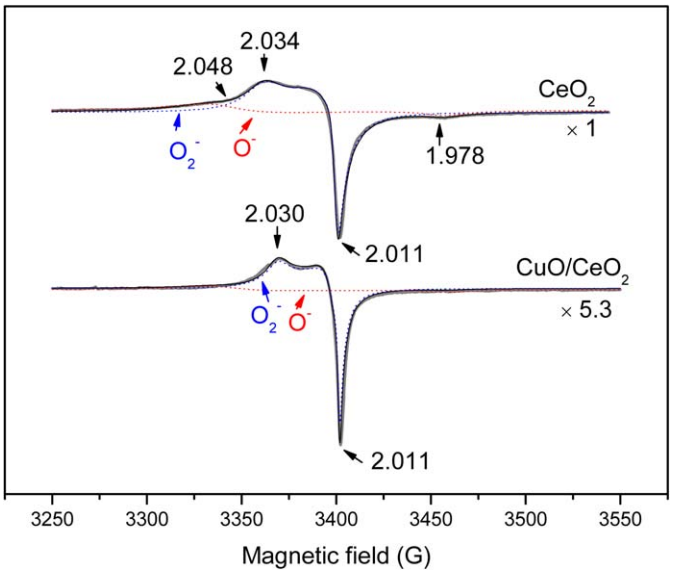

Fig. 1. EPR spectra at 77 K for the indicated samples after adsorption of a dose of ca. 50 μmol g^{-1} of O_2 at 77 K over the samples reduced under CO at 473 K. The experimental spectra are shown as thicker gray lines while simulation is overlapped as thinner black line. Components employed for the simulation are shown as dotted blue and red lines (see text for details).

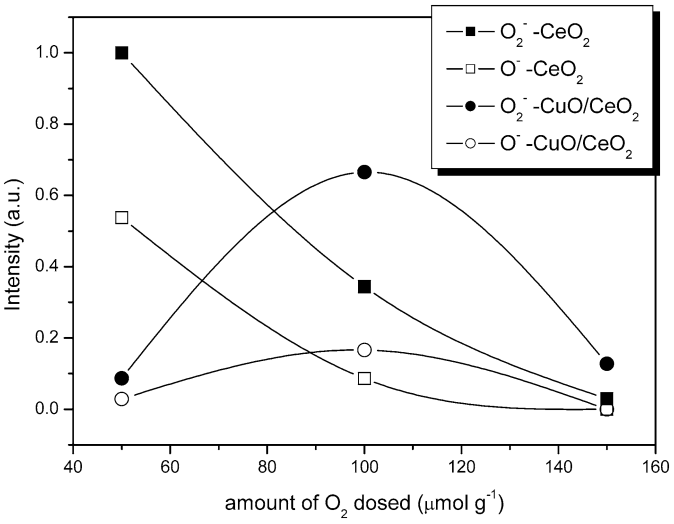

Fig. 2. Evolution of the intensities of superoxide and O^- species detected during the O_2-probe EPR spectra as a function of the amount of O_2 dosed at 77 K.

ried out isothermally at different temperatures (between room temperature and 773 K) using O_2/He or CO/He gas mixtures for the redox treatments at a flow rate of ∼20 mL min^{-1}.

3. Results and discussion

A first set of experiments consisted of EPR monitoring of oxygen radicals generated on low-temperature oxygen adsorption on the samples reduced under CO at 473 K; qualitative aspects of this study were reported previously, and are also included here for the sake of completeness [27]. Such an O_2-probe EPR method typically yields important information on the first stages of oxygen chemisorption, which for this type of material involves electron transfer from the reduced surface to the oxygen molecules [33,34]. For this particular case, to obtain a detailed picture of the oxidation process, an initial dose of oxygen is adsorbed at 77 K on the reduced sample, and the evolution of the oxygen radicals thus formed is followed after warming to room temperature in the closed cell. Then a second, a third, and so on, oxygen dose is chemisorbed in the same way (77 K → room temperature) to produce a gradual sample oxidation. The experiment is finished when no further changes are detected in the oxygen-derived signals (or they achieve a relatively weak intensity). EPR spectra after adsorption of the first oxygen dose at 77 K on the samples reduced under CO at 473 K are shown in Fig. 1. The spectra reveal the generation of two types of oxygen-derived radicals (with cerium cations acting as chemisorption centers in some cases, according to previous analyses [27,33,34]). The first type corresponds to superoxide species (O_2^- anions) [27,33,34], characterized by principal g components of $g_z = 2.034$–2.030, $g_x = 2.018$–2.014, and $g_y = 2.013$–2.011 (with axis assignments based on criteria described previously [33,34]); the second type is represented by a signal with a considerably broader line shape and principal g components of $g_\perp = 2.048$ and $g_{||} = 1.978$, being assigned to O^- anions [27,35]. Full details on the assignments made and characteristics of these signals have been given previously [27,33,34]. Subsequent warming to room temperature of the samples with oxygen adsorbed at 77 K (as in Fig. 1) causes disappearance of the oxygen-derived signals. Recovery of these signals to varying levels, as displayed in Fig. 2, occurs after adsorption of the second O_2 dose at 77 K. However, notwithstanding the amount of oxygen accumulatively dosed at 77 K (generating varying amounts of oxygen-derived radicals, as shown in Fig. 2), subsequent warming to room temperature in the closed cell always induces the disappearance of or a very strong decrease in such signals in all samples. This contrasts with results observed for samples mildly reduced under vacuum, in which the superoxide radicals were shown to be stable at room temperature [33]. Certainly, besides differences in the degree of reduction achieved in each case, modification of surface centers by carbonate formation during reduction under CO (in accordance with infrared results [not shown]) can account for these differences. The evolution shown in Fig. 2 is compatible with a gradual oxidation of the samples, which by the end of the oxidation process is practically unable to release any more electrons to the oxygen molecules. The main difference between the samples concerns the maximum detected in CuO/CeO_2 at intermediate dosing (Fig. 2). This can be related to the greater reducing power of this latter sample resulting from a copper-enhanced surface reducibility under CO [27]. This can lead to formation of mainly charged diamagnetic oxygen-derived species (like peroxide or oxide, resulting from multiple electron transfer processes, according to the discussion below) when the first oxygen dose is chemisorbed on the sample in its initial reduced state. Then single-electron transfers (leading to paramagnetic superoxide species) appears to be favored in this sample on oxygen adsorption at 77 K on the sample displaying an intermediate degree of oxidation of the surface (here achievable after room temperature adsorption of the first oxygen dose and according to the

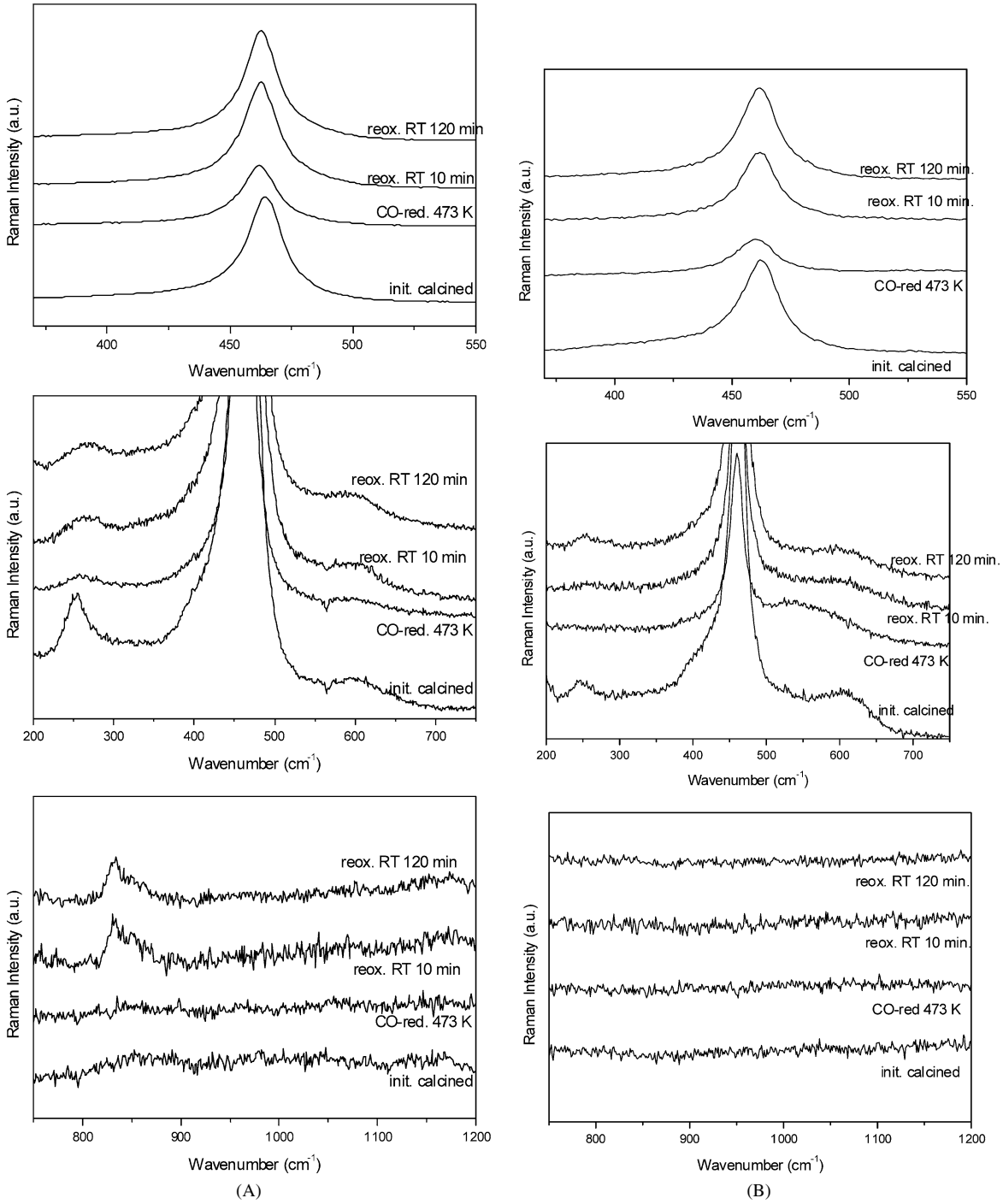

Fig. 3. (A) Raman spectra of CeO_2 at RT after the indicated redox treatments under diluted CO or O_2 flows. (B) The same for CuO/CeO_2.

maximum observed on adsorption of the second dose at 77 K; see Fig. 2).

To investigate the nature of the diamagnetic oxygen-derived species formed at room temperature (as revealed by the practical disappearance of all oxygen-derived signals in the EPR spectra, in contrast to adsorption at 77 K) on the interaction of the CO-reduced samples with O_2, the samples were investigated by in situ Raman spectroscopy. As shown in Fig. 3, the spectra of the initial calcined samples were dominated by a peak at ca. 462 cm^{-1} corresponding to the triply degenerate F_{2g} mode of fluorite CeO_2 (the only one allowed in first order). The main differences between the samples concern the position of the maximums of such peaks (464.3 cm^{-1} for CeO_2 and 461.9 cm^{-1} for CuO/CeO_2), their width (18.6 cm^{-1} FWHM for CeO_2 and 21.2 cm^{-1} FWHM for CuO/CeO_2, with the latter demonstrating somewhat greater asymmetry, related to a higher red half-width), and their intensity (higher for CeO_2). This has been interpreted in a previous work as being due mainly to a higher phonon confinement in CuO/CeO_2 as a consequence of a small copper incorporation into the ceria lattice (basically at

positions close to the ceria surface) [27]. This is supported by the somewhat higher relative intensity of a broad contribution centered at ca. 600 cm^{-1}, attributed to a second-order band associated with the presence of oxygen vacancies [36], observed for CuO/CeO_2. Keep in mind that the incorporation of copper into the fluorite ceria lattice must be accompanied by the formation of oxygen vacancies [37]. Another second-order peak, detected for both samples, was apparent at ca. 270 cm^{-1} [38]. Evolution of the spectra as a function of redox treatments, first under CO at 473 K and then subsequently under O_2 at room temperature, is shown in Fig. 3. Of note, apparent changes in the frequency of the F_{2g} mode occurred on such redox treatments (as shown in Fig. 4), while its width remained basically unchanged. In particular, the shift produced on CO reduction along with the apparent intensity reduction indicate, in line with XRD results (see below), an appreciable reduction of bulk ceria, because such a shift is characteristic of the presence of reduced cerium ions (formally Ce^{3+}) [25]. As shown in Figs. 3 and 4, the process was reversed on subsequent interaction with O_2 at room temperature, indicating an appreciable reoxidation of the samples. But a more complete oxidation appears to have been achieved for CuO/CeO_2 on the basis of the higher reversibility of the F_{2g} mode position (Fig. 4). In accordance with this finding, it is noteworthy that such oxidation apparently occurred without formation of incompletely reduced oxygen species (at least adsorbed superoxide or peroxide species, which are expected to be Raman active [39]) for the copper-containing catalyst. In contrast, the formation of peroxide species (O_2^{2-} giving bands at 831 and ca. 860 cm^{-1} [39]) was apparent for CeO_2. Note that the absence of superoxide species in the Raman spectra of these samples and the evolution of the corresponding spectra during these redox treatments explain the lack of paramagnetic radicals on contact of the CO-reduced sample with O_2 at room temperature in the EPR experiments. In turn, this indicates that this effect is independent of the degree of oxidation achieved by the samples prereduced under CO.

To complement these results, the samples were examined by in situ XRD under O_2/CO (using synchrotron-derived X-rays to optimize the signal-to-noise ratio). For both samples, the diffractograms show exclusively peaks corresponding to the fluorite structure of ceria. The absence of peaks due to copper-related phases in CuO/CeO_2 must be attributed to the high dispersion of copper in the sample also as a consequence of its relatively low copper content [27]; that is, the particles of CuO must be smaller than ca. 2 nm. Fig. 5 shows a typical series of diffractograms recorded for the CuO/CeO_2 sample. The main changes observed in the course of thermal treatments under O_2/CO are related to variations in the lattice parameter (Fig. 6). During the reduction process, two Ce^{4+} cations are reduced to two Ce^{3+} cations with one oxygen vacancy formed ($CO + 2Ce^{4+} + O^{2-} \rightarrow 2Ce^{3+} + V_{\ddot{O}} + CO_2$). Because Ce^{3+} is larger than Ce^{4+}, a simple reduction leads to a ceria lattice cell expansion [2,40,41]. Thus, changes in the lattice parameter can be directly correlated to the reduction of the cerium cations. In turn, a small lattice contraction would be expected if Cu^{2+} cations replaced Ce^{4+} cations in the ceria lattice as a consequence of balance between the smaller size of Cu^{2+} (leading to

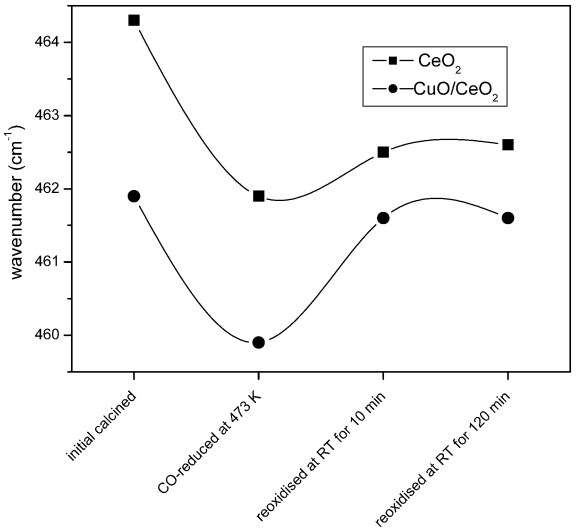

Fig. 4. Evolution of the Raman F_{2g} mode frequency as a function of the redox treatments performed.

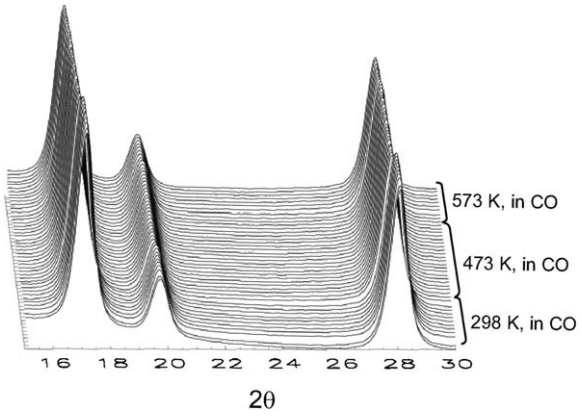

Fig. 5. Illustrative series of X-ray diffractograms recorded during thermal treatments under O_2/CO for the CuO/CeO_2 sample.

contraction) and generation of an oxygen vacancy (producing expansion) for charge compensation [37]. On this basis, differences between the lattice parameters of the initial samples reflect the fact that a small amount of copper was introduced in the ceria lattice during sample preparation, in agreement with previous investigations [27]. It is interesting that a slightly lower lattice parameter is observed at room temperature after treatment of any of the samples under oxygen at 773 K. This suggests that the initial samples (calcined under atmospheric air) can contain, as typically observed in nanostructured configurations of ceria [22–25], a small amount of reduced cerium that becomes oxidized during in situ treatment under diluted O_2. On the other hand, analysis of the evolution of the lattice parameter in the course of treatment under CO clearly demonstrates an appreciable reduction in the ceria lattice [2,42]. In particular, comparison of lattice parameters of the samples reduced under CO at 473 K with those reduced under O_2 at 773 K (the latter exclusively reflecting thermal expansion of the fully oxidized sample, with expansion values in agreement with previous investigations of nanostructured ceria and probably affected by strain relaxation during heating [25,26]) demonstrates that lat-

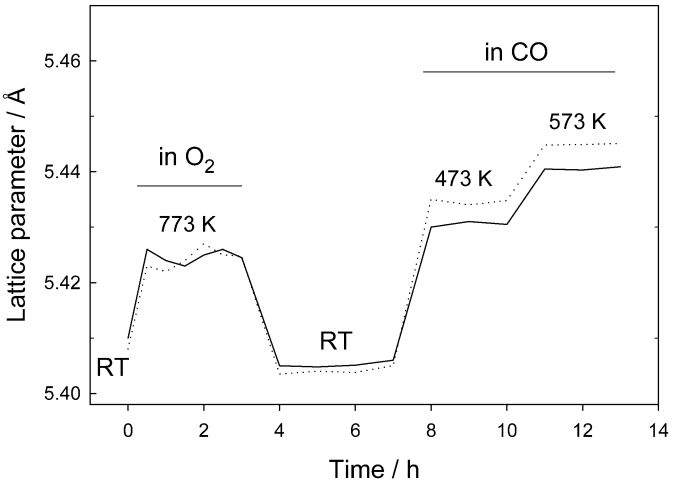

Fig. 6. Evolution of the fluorite lattice parameter during the indicated redox treatments for CeO_2 (solid trace) and 1%Cu/CeO_2 (dashed trace). The samples were exposed to O_2 at 773 K, then cooled to room temperature (RT), and finally exposed to CO at 473 and 573 K.

tice reduction was produced by the treatment under CO, thus giving support to the arguments advanced for interpretation of the Raman results (Figs. 3 and 4). Comparison between both samples reveals a small copper promotion of ceria reduction, in agreement with previous investigations [27]. An approximate estimation of the degree of reduction achieved on treatment under CO at 473 K for both samples can be made on the basis of the thermal expansion observed for the stoichiometric samples (ca. 4.25×10^{-5} Å K^{-1}, in fair agreement with results in the literature [40,42]; Fig. 6), and results available in the literature for the lattice expansion produced at different reduction degrees of ceria [42]. (Note also for this analysis that copper incorporation to the ceria lattice must be very small in the CuO/CeO_2 sample, according to previous reports [27,37].) According to this analysis, approximately 8 and 10% of the cerium would be reduced to Ce^{3+} under CO at 473 K in CeO_2 and CuO/CeO_2, respectively. Note that compared with earlier results, in which reduction of the ceria bulk under CO was claimed to occur at temperatures above 473 K [43], bulk reduction by CO may be favored by the nanostructured nature of the samples analyzed here, because this can enhance the oxygen mobility in these samples [21]. In this respect, an earlier report by Padeste et al. pointed out a bulk reducibility under CO on decreased crystallinity of ceria [44].

4. Conclusion

In summary, joint analysis of O_2-probe EPR and in situ Raman results (with the support of in situ XRD) gave a rather complete picture of the oxygen-handling properties of the samples. The reduction of external oxygen leading to reoxidation of the samples is usually assumed to follow the scheme $O_2 \leftrightarrow O_2^- \leftrightarrow O_2^{2-} \leftrightarrow 2O^- \leftrightarrow 2O^{2-}$ [35]. Within this scheme, observation of O^- species by EPR (Figs. 1 and 2) revealed that oxygen can be readily dissociated on interaction at 77 K with the CO-reduced samples. This finding, along with the relatively high reducing power of the CO-reduced sample, makes it difficult to precisely control the initial steps in the electron transfer process leading to formation of superoxide species (on transfer of a single electron), thus limiting the use of this O_2-probe EPR technique in titrating the reduced surface for such a reduced sample state [34]. Nevertheless, the evolution of O^- and O_2^- as a function of the amount of oxygen dosed (Fig. 2) were consistent with a gradual loss of reductive power of the samples as they achieve higher degrees of oxidation. On the other hand, whereas rather complete oxidation of both samples was achieved on O_2 interaction at room temperature (i.e., oxygen must evolve mainly toward the formation of oxide anions, according to EPR and Raman), the Raman experiments of Figs. 3 and 4 indicate that copper facilitates completion of the redox process. This must be attributed, according to recent investigations [27,37], to the particular properties of the interfacial CuO–CeO_2 sites present in the catalyst. Such a role of copper can be relevant in explaining the remarkable activity of this system in oxidation reactions [5–14,16,17]. A similar promoting role has been recently proposed for gold in systems supported on IrO_2/TiO_2 [45]. In turn, the results obtained with the different techniques suggest a limited role for partially reduced oxygen species (superoxide or peroxide) on the CO oxidation activity of CuO/CeO_2 at temperatures of relevancy for this process (say, between 300 and 450 K [7,17]).

Acknowledgments

Thanks are due to S.J. Khatib and M.A. Bañares for their help in recording Raman spectra. D.G. thanks the FPI program of the "Ministerio de Educación y Ciencia" for a doctoral research grant. Financial support from CICYT project MAT2003-03925 is acknowledged. The research carried out at Brookhaven National Laboratory was financed through contract DE-AC02-98CH10086 with the U.S. Department of Energy, Division of Chemical Sciences.

References

[1] A. Trovarelli, Catal. Rev. Sci. Eng. 38 (1996) 439.
[2] A. Trovarelli, in: A. Trovarelli (Ed.), Catalysis by Ceria and Related Materials, Catalytic Science Series, vol. 2, Imperial College Press, London, 2002, p. 15, and references therein.
[3] E.P. Murray, T. Tsai, S.A. Barnett, Nature 400 (1999) 649.
[4] S. Park, J.M. Vohs, R.J. Gorte, Nature 404 (2000) 265.
[5] W. Liu, A.F. Sarofim, M. Flytzani-Stephanopoulos, Chem. Eng. Sci. 49 (1994) 4871.
[6] M.-F. Luo, Y.-J. Zhong, X.-X. Yuan, X.-M. Zheng, Appl. Catal. A 162 (1997) 121.
[7] A. Martínez-Arias, M. Fernández-García, O. Gálvez, J.M. Coronado, J.A. Anderson, J.C. Conesa, J. Soria, G. Munuera, J. Catal. 195 (2000) 207.
[8] G. Avgouropoulos, T. Ioannides, Ch. Papadopoulou, J. Batista, S. Hočevar, H.K. Matralis, Catal. Today 75 (2002) 157.
[9] P. Ratnasamy, D. Srinivas, C.V.V. Satyanarayana, P. Manikandan, R.S.S. Kumaran, M. Sachin, V.N. Shetti, J. Catal 221 (2004) 455.
[10] D.H. Kim, D.E. Cha, Catal. Lett. 86 (2003) 107.
[11] J.B. Wang, S.-C. Lin, T.-J. Huang, Appl. Catal. A 232 (2002) 107.
[12] Y. Liu, T. Hayakawa, T. Tsunoda, K. Suzuki, S. Hamakawa, K. Murata, R. Shiozaki, T. Ishii, M. Kumagai, Top. Catal. 22 (2003) 205.
[13] W.-J. Shen, Y. Ichihashi, Y. Matsumura, Catal. Lett. 79 (2002) 125.
[14] Q. Fu, S. Kudriatseva, H. Saltsburg, M. Flytzany-Stephanopoulos, Chem. Eng. J. 93 (2003) 41.

[15] X. Wang, J.A. Rodriguez, J.C. Hanson, D. Gamarra, A. Martínez-Arias, M. Fernández-García J. Phys. Chem. B 110 (2006) 428.
[16] G. Sedmak, S. Hočevar, J. Levec, J. Catal. 222 (2004) 87.
[17] A. Martínez-Arias, A.B. Hungría, M. Fernández-García, J.C. Conesa, G. Munuera, J. Power Sources 151 (2005) 32.
[18] S. Carrettin, P. Concepción, A. Corma, J.M. López Nieto, V.F. Puntes, Angew. Chem. Int. Ed. 43 (2004) 2538.
[19] K. Zhou, X. Wang, X. Sun, Q. Peng, Y. Li, J. Catal. 229 (2005) 206.
[20] A.B. Hungría, M. Fernández-García, J.A. Anderson, A. Martínez-Arias, J. Catal. 235 (2005) 262.
[21] M. Fernández-García, A. Martínez-Arias, J.C. Hanson, J.A. Rodríguez, Chem. Rev. 104 (2004) 4063.
[22] S. Tsunekawa, K. Ishikawa, Z.-Q. Li, Y. Kawazoe, A. Kasuya, Phys. Rev. Lett. 85 (2000) 3440.
[23] L. Wu, H.J. Wiesmann, A.R. Moodenbaugh, R.F. Klie, Y. Zhu, D.Q. Welch, M. Suenaga, Phys. Rev. B 69 (2004) 125415.
[24] F. Zhang, P. Wang, J. Koberstein, S. Khalid, S.-W. Chan, Surf. Sci. 563 (2004) 74.
[25] J.E. Spanier, R.D. Robinson, F. Zhang, S.-W. Chan, I.P. Herman, Phys. Rev. B 64 (2001) 245407.
[26] X.Q. Wang, J.C. Hanson, G. Liu, J.A. Rodriguez, A. Iglesias-Juez, M. Fernández-García, J. Chem. Phys. 121 (2004) 5434.
[27] A. Martínez-Arias, A.B. Hungría, M. Fernández-García, J.C. Conesa, G. Munuera, J. Phys. Chem. B 108 (2004) 17983.
[28] A. Martínez-Arias, M. Fernández-García, V. Ballesteros, L.N. Salamanca, J.C. Conesa, C. Otero, J. Soria, Langmuir 15 (1999) 4796.
[29] M.D. Hernández-Alonso, A.B. Hungría, A. Martínez-Arias, J.M. Coronado, J.C. Conesa, J. Soria, M. Fernández-García, Phys. Chem. Chem. Phys. 6 (2004) 3524.
[30] X.Q. Wang, J.C. Hanson, A.I. Frenkel, J.-Y. Kim, J.A. Rodriguez, J. Phys. Chem. B 108 (2004) 13667.
[31] P.J. Chupas, M.F. Ciraolo, J.C. Hanson, C.P. Grey, J. Am. Chem. Soc. 123 (2001) 1694.
[32] A.P. Hammersely, S.O. Svensson, A. Thompson, Nucl. Instrum. Methods Phys. Res. 346 (1994) 321.
[33] J. Soria, A. Martínez-Arias, J.C. Conesa, J. Chem. Soc., Faraday Trans. 91 (1995) 1669.
[34] J.C. Conesa, M. Fernández-García, A. Martínez-Arias, in: A. Trovarelli (Ed.), Catalysis by Ceria and Related Materials, Catalytic Science Series, vol. 2, Imperial College Press, London, 2002, p. 169.
[35] M. Che, A.J. Tench, Adv. Catal. 31 (1982) 77.
[36] J.R. McBride, K.C. Hass, B.D. Poindexter, W.H. Weber, J. Appl. Phys. 76 (1994) 2435.
[37] X. Wang, J.A. Rodríguez, J.C. Hanson, D. Gamarra, A. Martínez-Arias, M. Fernández-García, J. Phys. Chem. B 109 (2005) 19595.
[38] W.H. Weber, K.C. Hass, J.R. McBride, Phys. Rev. B 48 (1993) 178.
[39] V.V. Pushkarev, V.I. Kovalchuk, J.L. d'Itri, J. Phys. Chem. B 108 (2004) 5341.
[40] M. Fernández-García, X.Q. Wang, C. Belver, A. Iglesias-Juez, J.C. Hanson, J.A. Rodriguez, Chem. Mater. 17 (2005) 4181.
[41] X.Q. Wang, J.C. Hanson, J.A. Rodriguez, C. Belver, M. Fernández-García, J. Chem. Phys. 122 (2005) 154711.
[42] M. Mogensen, in: A. Trovarelli (Ed.), Catalysis by Ceria and Related Materials, Catalytic Science Series, vol. 2, Imperial College Press, London, 2002, p. 453, and references therein.
[43] A. Badri, J. Lamotte, J.C. Lavalley, A. Laachir, V. Perrichon, O. Touret, G.N. Sauvion, E. Quemere, Eur. J. Solid State Inorg. Chem. 28 (1991) 445.
[44] C. Padeste, N.W. Cant, D.L. Trimm, Catal. Lett. 18 (1993) 305.
[45] Z.-P. Liu, S.J. Jenkins, D.A. King, Phys. Rev. Lett. 93 (2004) 156102.